





Characterization of PM_{2.5} and PM₁₀ fugitive dust source profiles in the Athabasca Oil Sands Region

Xiaoliang Wang, Judith C. Chow, Steven D. Kohl, Kevin E. Percy, Allan H. Legge & John G. Watson


To cite this article: Xiaoliang Wang, Judith C. Chow, Steven D. Kohl, Kevin E. Percy, Allan H. Legge & John G. Watson (2015) Characterization of PM_{2.5} and PM₁₀ fugitive dust source profiles in the Athabasca Oil Sands Region, Journal of the Air & Waste Management Association, 65:12, 1421-1433, DOI: [10.1080/10962247.2015.1100693](https://doi.org/10.1080/10962247.2015.1100693)

To link to this article: <https://doi.org/10.1080/10962247.2015.1100693>

 View supplementary material [↗](#)


 Published online: 25 Nov 2015.

 Submit your article to this journal [↗](#)

 Article views: 2939

 View related articles [↗](#)

 View Crossmark data [↗](#)

 Citing articles: 12 View citing articles [↗](#)

Characterization of PM_{2.5} and PM₁₀ fugitive dust source profiles in the Athabasca Oil Sands Region

Xiaoliang Wang,^{1,3,*} Judith C. Chow,^{1,2,3} Steven D. Kohl,¹ Kevin E. Percy,⁴ Allan H. Legge,⁵ and John G. Watson^{1,2,3}

¹Desert Research Institute, Reno, NV, USA

²State Key Laboratory of Loess and Quaternary Geology, Institute of Earth Environment, Chinese Academy of Sciences, Xi'an, Shaanxi, People's Republic of China

³Graduate Faculty, University of Nevada, Reno, NV, USA

⁴Wood Buffalo Environmental Association, Fort McMurray, Alberta, Canada

⁵Biosphere Solutions, Calgary, Alberta, Canada

*Address correspondence to Xiaoliang Wang, Desert Research Institute, 2215 Raggio Parkway, Reno, NV 89512, USA; e-mail: xiaoliang.wang@dri.edu

Geological samples were collected from 27 representative locations in the Athabasca Oil Sands Region (AOSR) in Alberta, Canada. These samples were resuspended onto filter substrates for PM_{2.5} and PM₁₀ size fractions. Samples were analyzed for 229 chemical species, consisting of elements, ions, carbon, and organic compounds. These chemical species are normalized to gravimetric mass to derive individual source profiles. Individual profiles were grouped into six categories typical of those used in emission inventories: paved road dust, unpaved road dust close to and distant from oil sand operations, overburden soil, tailings sands, and forest soils. Consistent with their geological origin, the major components are minerals, organic and elemental carbon, and ions. The sum of five major elements (i.e., Al, Si, K, Ca, and Fe) and their oxidized forms account for 25–40% and 45–82% of particulate matter (PM) mass, respectively. Si is the most abundant element, averaging 17–18% in the Facility (oil sand operations) and 23–27% in the Forest profiles. Organic carbon is the second most abundant species, averaging 9–11% in the Facility and 5–6% in the Forest profiles. Elemental carbon abundance is 2–3 times higher in Facility than Forest profiles. Sulfate abundance is ~7 times higher in the Facility than in the Forest profiles. The ratios of cation/anion and base cation (sum of Na⁺, Mg²⁺, K⁺, and Ca²⁺)/nitrogen- and sulfur-containing ions (sum of NH₄⁺, NO₂⁻, NO₃⁻, and SO₄²⁻) exceed unity, indicating that the soils are basic. Lead (Pb) isotope ratios of facility soils are similar to the AOSR stack and diesel emissions, while those of forest soils have much lower ²⁰⁶Pb/²⁰⁷Pb and ²⁰⁸Pb/²⁰⁷Pb ratios. High-molecular-weight n-alkanes (C₂₅–C₄₀), hopanes, and steranes are more than an order of magnitude more abundant in Facility than Forest profiles. These differences may be useful for separating anthropogenic from natural sources of fugitive dust at receptors.

Implications: Several organic compounds typical of combustion emissions and bitumen are enriched relative to forest soils for fugitive dust sources near oil sands operations, consistent with deposition uptake by biomonitors. AOSR dust samples are alkaline, not acidic, indicating that potential acid deposition is neutralized. Chemical abundances are highly variable within emission inventory categories, implying that more specific subcategories can be defined for inventory speciation.

Introduction

Fugitive dust is among the largest fractions of PM_{2.5} and PM₁₀ (particles with aerodynamic diameter less than 2.5 μm and 10 μm, respectively) emissions in Alberta, Canada, with an estimate of ~39–46% from unpaved roads, ~43–49% from construction, and ~3–8% from agricultural activities (Environment Canada, 2014). With increased oil production in the Athabasca Oil Sands Region (AOSR) of northeastern Alberta, ~715 km² of land was affected as of 2012 by mining and upgrading operations, although current practices are reducing that footprint by requiring reclamation of mined-out areas

prior to excavating new areas (Stringham, 2012). Alberta mine tailings were estimated to emit 16 and 66 metric tons of PM_{2.5} and PM₁₀, respectively, in 2013 (Environment Canada, 2014). Other fugitive dust sources include unpaved roads and parking lots, construction of roads and buildings, and wintertime application of deicing material. Large dust plumes are often visible over disturbed land when wind speeds are high or when vehicles are moving on unpaved roads (Dowdeswell et al., 2010; Kunzig, 2009; Weinhold, 2011).

Resuspended dust is more than a nuisance due to potential adverse effects on air and water quality, ecosystems, and human health (Morman and Plumlee, 2013). Past studies on

river water, snowpack, and lichens show elevated abundances of polycyclic aromatic hydrocarbons (PAHs) and trace elements at locations near oil sands facilities (Addison and Puckett, 1980; Kelly et al., 2009; 2010). The extent to which these contaminants result from natural and anthropogenic sources, and their apportionment to area, mobile, and stationary emitters, are uncertain. Enrichments of fugitive dust markers (e.g., aluminum [Al]) and industrial process markers (e.g., vanadium [V]) in lichens achieve background levels within ~20 km of the main surface mining activities (Graney et al., 2012). Similarly, PAH concentrations measured in lichen samples have a smaller spatial footprint than elevated stack emissions (Studabaker et al., 2012). This is consistent with ground-level emissions of larger particles (with high deposition velocities) typical of fugitive dust. Landis et al. (2012) estimated that fugitive dust was the largest contributor to elemental concentrations in lichen samples near oil sands mining activities, with ~23% from the combustion process, ~19% from tailings sands, ~15% each from mine haul roads and limestone, oil sands and processed materials, and other anthropogenic urban sources.

The mineral components of fugitive dust source profiles can be distinguished from nongeological sources such as vehicle exhaust, biomass burning, and industrial emissions by their element, ion, and carbon abundances (Chow and Watson, 2002). However, because many species are common to and abundant in all fugitive dust emitters, elements, ions, and carbon fractions are not sufficient to distinguish many different fugitive dust source contributions from one another. The composition of the suspendable fugitive dust in the AOSR represents a mixture of native soil with deposited engine exhaust, brake and tire wear, stationary source emissions, plant detritus and other biological material, tailings sands, and mined or naturally occurring bitumen. Landis et al. (2012) found collinearities among AOSR fugitive dust profiles that contained only elemental abundances. Extending chemical analyses to more species, including particle-phase PAHs, can potentially break these collinearities using source apportionment receptor models (Watson and Chow, 2015). These profiles are also needed to create speciated emission inventories (e.g., Gargava et al., 2014) for source-oriented dispersion modeling to better evaluate effects of current and future emissions and to target effective emission reduction strategies.

Herein are reported PM_{2.5} and PM₁₀ source profile abundances (mass fraction of each measured species) for 27 fugitive dust samples acquired in the AOSR, including those from paved roads and shoulders, unpaved roads within and outside of mining facilities, surface soil from mining pits, sands from tailings pond dikes, mine overburden soil, and bare forest soil. Mass abundances were measured for 229 chemical components, including elements (sodium [Na] to uranium [U]), rare earth elements, lead (Pb) isotopes, ions, organic and elemental carbon (OC and EC), nonpolar organic compounds, carbohydrates, organic acids, and water-soluble organic carbon (WSOC). Objectives of this study are to (1) document the sources, sampling methods, and chemical analyses; and (2) examine similarities and differences in chemical components among PM_{2.5} and PM₁₀ size fractions for the sampled surfaces.

Materials and Methods

Sampling sites and sample collection

Table 1 summarizes the sampling locations (also shown in the map in supplemental Figure S-1) and soil characteristics. Samples were collected from four mining and upgrading facilities (i.e., Facilities A–D in Table 1) and in the surrounding areas, including jack pine forests located north and northwest of the facilities.

For paved/unpaved road and highway shoulders, loose surface material was swept with a clean whisk broom into a dustpan. For bulk sands and soils, grab samples were collected with a small garden spade to a depth of 10 to 15 cm from the surface. Each sample (~1–1.5 kg) was a composite of dust from several locations on a surface that were homogenized in double-sealed polyethylene bags prior to resuspension. Sampling equipment was cleaned after collection at each surface.

Laboratory resuspension and chemical analyses

Samples were air dried (~25°C) in the laboratory for ~1 week, then sieved through a Tyler 400 mesh screen (~38.5 μm in geometric diameter). Approximately 1–10 g of the sieved material was puffed into a laboratory resuspension chamber (Chow et al., 1994) and sampled through PM_{2.5} and PM₁₀ size-selective inlets onto six parallel channels of filter packs (Figure S-2), including one Teflon-membrane filter (Teflo R2PJ047, Pall Corporation, Ann Arbor, MI) and two quartz-fiber (Tissuquartz, 2500 QAT-UP, Pall Corporation, Ann Arbor, MI) filters for each size fraction. Concentrations within the chamber were monitored to achieve optimal loadings of 1–3 mg/filter for analyses.

Blank and exposed Teflon-membrane filters were equilibrated in a clean room with controlled temperature (21.5 ± 1.5°C) and relative humidity (RH, 35 ± 5%) for >24 hr before mass determination by gravimetry, per U.S. Environmental Protection Agency (EPA) (1997) specifications. Filters were weighed before and after sampling with a ±1-μg sensitivity microbalance (XP6, Mettler Toledo Inc., Hightstown, NJ). Teflon-membrane filters were analyzed for 51 elements (from Na to U) by high-sensitivity energy-dispersive x-ray fluorescence (XRF; Panalytical Epsilon 5, Almelo, The Netherlands) (Watson et al., 1999). The same filters were then submitted for acid digestion in a hot block digester and analyzed for cesium (Cs), barium (Ba), 14 rare earth elements, and four Pb isotopes (i.e., ²⁰⁴Pb, ²⁰⁶Pb, ²⁰⁷Pb, and ²⁰⁸Pb) by inductively coupled plasma/mass spectrometry (ICP/MS; Thermo Electron X series, Madison, WI) (Komárek et al., 2008; Ohno and Hirata, 2004).

Quartz-fiber filters were pre-fired at 900°C for 4 hr to remove organic artifacts prior to laboratory resuspension. Half of the first quartz-fiber filter was extracted in distilled-deionized water (DDW) and analyzed for (1) anions (i.e., chloride [Cl⁻], nitrite [NO₂⁻], nitrate [NO₃⁻], phosphate [PO₄³⁻], and sulfate [SO₄²⁻]) by ion chromatography (IC; Dionex ICS-3000, Sunnyvale, CA) (Chow and Watson, 1999); (2) water-soluble cations (i.e., sodium [Na⁺], magnesium [Mg²⁺], potassium [K⁺], and calcium [Ca²⁺]) by atomic absorption spectroscopy

Table 1. Description of fugitive dust samples from the Athabasca Oil Sands Region (AOSR), Alberta, Canada.

Fugitive dust emission category	Site ID	Site location	Description	Sample date	Latitude/longitude		Profile mnemonic	Facility Forest grouping
					N	W		
Paved road dust	S6	Facility B	Paved mine haul road dust (near intersection with unpaved mine haul road)	10/1/2008	57.26575	-111.51800	PRd	Facility
Unpaved road dust (Facility)	S17	Highway 63	Shoulder dust of south bound lane	10/2/2008	56.85960	-111.44364	PRd	Facility
	S1	Facility A	Mine haul road dust	10/3/2008	57.32124	-111.48168	OUPRd	Facility
	S3	Facility A	Ramp soil to tailings pond	10/3/2008	57.32029	-111.45376	OUPRd	Facility
	S5	Facility B	Unpaved mine haul road dust (north side of mine)	10/1/2008	57.27247	-111.50313	OUPRd	Facility
	S7	Facility B	Tailings haul road dust	10/1/2008	57.23978	-111.53803	OUPRd	Facility
	S9	Facility B	Ramp soil to tailings pond dike	10/1/2008	57.24455	-111.56739	OUPRd	Facility
	S10	Facility B	Road dust on top of tailings pond dike	10/1/2008	57.24455	-111.56739	OUPRd	Facility
	S13	Facility C	Dirt road soil on dike	10/2/2008	57.05368	-111.63205	OUPRd	Facility
	S14	Facility C	Ramp soil to tailings pond dike	10/2/2008	57.05238	-111.62570	OUPRd	Facility
	S16	Facility D	Tailings haul road dust	10/2/2008	56.99520	-111.49988	OUPRd	Facility
Unpaved road dust	S25	100S174	Surface soil off dirt road (to Ft Chipewyan) surface	8/26/2008	57.64321	-111.19102	FUPRd	Forest
Tailings sands	S4	Facility A	Tailings dike (white sand)	10/3/2008	57.32191	-111.44904	TSand	Facility
	S8	Facility B	Drifting sand on tailings pond dike	10/1/2008	57.23771	-111.54086	TSand	Facility
	S11	Facility B	Drifting sand along tailings line on top of dike	10/1/2008	57.24455	-111.56739	TSand	Facility
	S12	Facility B	Tailings pond dike sand	10/1/2009	57.26380	-111.50896	TSand	Facility
	S15	Facility D	Drifting sand along tailings line on pond 2/3	10/2/2008	56.99299	-111.50089	TSand	Facility
Overburden soil	S2	Facility A	Mine overburden area soil	10/3/2008	57.34177	-111.47864	OB	Facility
	S18	15B4	Disturbed sandy soil from an excavated pit	9/20/2008	56.96142	-111.57554	FSoil	Forest
Forest soil	S19	15B5	Mixture of surface soil from road and overburden from ditch construction	9/18/2008	57.02596	-111.77355	FSoil	Forest
	S20	30B25	Well pad surface soil downwind of a 2007 fire	9/20/2008	56.97113	-111.97471	FSoil	Forest
Forest soil	S21	30B16	Pipeline excavation soil	8/29/2008	57.19693	-111.44426	FSoil	Forest
	S22	30B11	Pipeline excavation soil, unhealthy lichen	8/26/2008	57.05068	-111.18442	FSoil	Forest
	S23	65S137	Exposed soil on the water ditch	8/25/2008	57.40345	-111.07497	FSoil	Forest
	S24	100S168	Well pad surface soil	8/26/2008	57.69236	-111.05690	FSoil	Forest
	S26	150AC69	Sandy soil at base of unburned tree root	8/14/2008	57.44784	-109.96739	FSoil	Forest
	S27	150B2	Surface soil on upslope of a ridge facing mining operation	8/19/2008	58.09669	-111.10163	FSoil	Forest

Note: Source type mnemonics: PRd—paved road dust; OUPRd—oil sands unpaved road dust; FUPRd—forest unpaved road dust; TSand—tailings sand; OB—overburden; and FSoil—forest soil.

(AAS; Varian Spectro880, Walnut Creek, CA) (Butler et al., 2009; Fernandez, 1989); (3) ammonium (NH_4^+) by automated colorimetry (AC; Astoria 302A Colorimetry System, Astoria, OR) (Fung et al., 1979); (4) 16 carbohydrates by IC with pulse amperometric detectors (PAD) (Engling et al., 2006); (5) 9 organic acids (sum of both dissociated and non-dissociated organic forms) by IC with conductivity detector (Jaffrezo et al., 1998); and (6) WSOC by a total organic carbon analyzer (TOC, Shimadzu, Columbia, MD) (Decesari et al., 2000).

Punches of $\sim 0.5 \text{ cm}^2$ were removed from the second quartz-fiber filters to quantify OC, EC, and eight thermal fractions (OC1–OC4, pyrolyzed carbon [OP], and EC1–EC3) by the IMPROVE_A thermal/optical protocol (model 2001, Atmoslytic, Inc., Calabasas, CA) (Chow et al., 1993, 2007a, 2011). Carbonate carbon ($\text{CO}_3^{2-}\text{-C}$) was determined by acidification with 15 μl of 0.4 M hydrochloride solution prior to carbon analyses. Approximately 1–2 cm^2 of each quartz-fiber filter was analyzed for 113 nonpolar organic compounds, including 26 *n*-alkanes ($\text{C}_{15}\text{--C}_{40}$), 10 iso/anteiso-alkanes ($\text{C}_{29}\text{--C}_{33}$), 2 methyl alkanes, 3 branched alkanes, 5 cycloalkanes, 36 PAH compounds, 18 hopanes, 12 steranes, and 1 alkene, by thermal desorption–gas chromatography/mass spectrometry (TD-GC/MS; model 6890N, Agilent Technology, Foster City, CA; see Figure S-2 for detailed compounds) (Chow et al., 2007b; Ho and Yu, 2004).

Results and Discussion

Mass abundances (percent by weight) and their analytical uncertainties (Watson et al., 2001) for the $\text{PM}_{2.5}$, PM_{10} , and $\text{PM}_{10-2.5}$ ($\text{PM}_{\text{coarse}}$) fractions for each sample are reported in spreadsheet form in supplemental Table S-1. Because compositing profiles by source type might mask important differences between samples from similar sources, the individual profiles in Table S-1 allow users to select the profiles of interest and composite the profiles for specific applications. Abundances lower than instrumental minimum detection limits are highlighted in these spreadsheets, and the associated uncertainty can be used as an upper limit for the abundance. This is useful when making speciated emission comparisons among different source types such as diesel exhaust. Abundances for several of the more prominent chemical components are graphically compared in supplemental Figures S-3 through S-12, except for Figure S-8.

Individual profile abundances were averaged by emission inventory source category and assigned mnemonics (i.e., PRd—paved road dust; OUPRd—oil sands unpaved road dust; FUPRd—forest unpaved road dust; TSand—tailings sand; OB—overburden; and FSoil—forest soil), as designated in Table 1, to obtain composite profiles that are detailed in Table S-2. Uncertainties associated with these abundances in Table S-2 are the larger of the analytical uncertainty or the standard deviation of the abundances included in the average. Average abundances and uncertainties for the composite Facility and Forest profiles (Table S-3) were calculated for samples taken close to and distant from oil sands operations, respectively; the individual profiles included in each of these

are indicated in the last column of Table 1. Although the abundances have large uncertainties in these two composites, they offer the opportunity to examine enrichments in measured species over those found in natural soils. Minimum detection limits for the measured species are listed in Table S-4. Similarities and differences between the $\text{PM}_{2.5}$ profiles are documented in Tables S-5 to S-7.

Figure 1 provides an overview of the major components in each profile. The sum of measured species (excluding double counting for P and PO_4^{3-} , S and SO_4^{2-} , Cl and Cl^- , K and K^+ , and Ca and Ca^{2+}) accounts for 35–70% of PM mass. Less than 100% of the gravimetric mass is expected as oxygen (O) and/or hydrogen (H) associated with OC and minerals are not measured. Reconstructed mass (Chow et al., 2015) accounts for $96 \pm 8\%$ (range 83–110%) of $\text{PM}_{2.5}$ and $87 \pm 9\%$ (range 74–110%) of PM_{10} . On average, $\text{PM}_{2.5}$ constitutes 23.9 \pm 6.7% of PM_{10} , which is similar to ratios found elsewhere (Chow et al., 2003; Vega et al., 2001; Wu et al., 2011).

Major chemical components

Geological minerals (assumed to be in the forms of Al_2O_3 , SiO_2 , K_2O , CaO , and Fe_2O_3) are the major components, accounting for 45–82% of particulate matter (PM) mass. Silicon dioxide (SiO_2) is the most abundant mineral oxide, explaining 24–75% of PM mass. Organic matter (OM) is calculated as $1.8 \times \text{OC}$, consistent with the multiplier used for the Interagency Monitoring of Protected Visual Environments (IMPROVE) network (Pitchford et al., 2007). OM/OC ratios for ambient PM vary from 1.2 for fresh combustion emissions in urban areas to 2.6 for aged PM. The actual multiplier may be larger if it is associated with lignin, cellulose, and humic-like substances (HULIS) that are often found in soil samples (Cannon and Anderson, 1991; Graber and Rudich, 2006; Schulten and Leinweber, 2000). A Van Bemmelen's factor of 1.724 has historically been used to estimate soil OM from OC, although Pribyl (2010) found 1.9–2.0 multipliers to be more accurate. OM is the second most abundant fugitive dust component after minerals, but with large site-to-site variations (with 45% coefficient of variation [CV]).

Elemental abundances

The five most abundant (>1% of PM) mineral-related elements (i.e., Al, Si, K, Ca, and Fe) account for 25–40% of PM mass in all profiles. Silicon (Si) abundances in the composite profiles (Figure 2) are lowest for PRd and OUPRd (15–17%), higher for TSand and OB soil (17–21%), and highest for FSoil (24–28%). This is reflected in the comparison of the Forest (23–27%) and Facility (17–18%) profiles. Aluminum (Al) abundances show the opposite: lower in the Fsoil (1.6–2.2%), higher in the OUPRd (4–5%), and highest in the TSand (5–6%) profiles. Potassium (K) abundances in the individual profile are in the range of 0.5–1.9%, shown in Figure S-3. Total K is 10–24 times that of water-soluble K^+ . This is consistent with past observations for dust samples (Chow et al., 2003; 2004; Han et al., 2007; Ho et al., 2003; Vega et al., 2001), except when they contain biomass burning residues (Andreae, 1983).

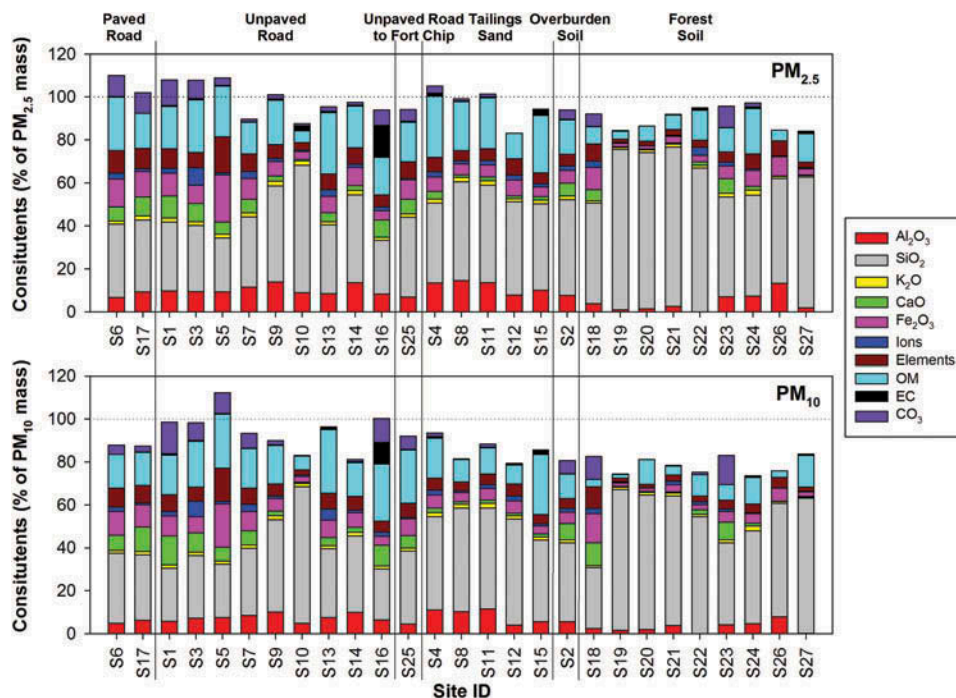


Figure 1. PM_{2.5} and PM₁₀ mass reconstruction (Chow et al., 2015) of major components in each fugitive dust profile: (1) Metal oxides include: Al₂O₃ = 1.89[Al]; SiO₂ = 2.14[Si]; K₂O = 1.21[K]; CaO = 1.4[Ca]; and Fe₂O₃ = 1.43[Fe]; (2) ions are the sum of Cl⁻, NO₂⁻, NO₃⁻, PO₄³⁻, SO₄²⁻, Na⁺, Mg²⁺, and NH₄⁺; (3) elements are the sum of elements (see Supplemental Table S-1), excluding Na, Mg, Al, Si, Cl, K, Ca, Fe, P in PO₄³⁻, and S in SO₄²⁻; (4) organic matter (OM) = 1.8 × organic carbon (OC); (5) EC = elemental carbon; and (6) carbonate = CO₃²⁻. Specific organic compounds are assumed to be included in OC. See Table 1 for site ID.

The calcium (Ca) abundance is variable among profiles (0.1–10%), with a maximum of 10% in PM₁₀ for S1 (Figure S-3). The composite profiles in Figure 2 show that TSand contains the lowest Ca abundance (~1%)—much less than the PRd abundances (~6–7%). The high PRd Ca abundances result in a factor of 2 enrichment in Facility (3–4%) over Forest (1.7–2%) profiles. Iron (Fe) abundances range from 1–15% in the individual profiles (Figure S-3), with the highest abundances in paved (e.g., S6 and S17) and unpaved (e.g., S1, S5, S7) road samples; this is consistent with contributions from metal, brake, and clutch wear (Pant and Harrison, 2013; Thorpe and Harrison, 2008). Fe abundances are low in the composite TSand, OB, and FSoil profiles (3–4%), ~half of those for PRd (7.5–9%).

Other detected elements, shown in Figure S-4 and S-5, have low abundances (0.0001% to <1% on average). V (Figure S-5) is more abundant in road dust (e.g., S1, S3, S5–S7, S9, S16, and S25), possibly due to exhaust deposition (Shafer et al., 2012) and V-rich bitumen and coke trackout (Jacobs and Filby, 1982; Puttaswamy and Liber, 2012; Shafer et al., 2012). Table S-2 shows that V is not enriched in the TSand profile. Titanium (Ti) and zirconium (Zr) can be enriched (Ciu et al., 2003) in froth treatment tailings (as high as 6.54% and 2.7% of mass, respectively). Elevated Ti (~0.6%) and Zr (~0.03%) abundances are found in the TSand profile. Chromium (Cr, 0.4–0.7%) and nickel (Ni, 0.2–0.3%) abundances are similar among the tailings pond sands, with S12 from Facility B (Figure S-4) having the highest abundance.

Organic and elemental carbon abundances

There are large site-to-site variations in OC abundances, ranging from 1 to 13% (with 53% CV) for forest soils (S18–S27) and from 7 to 17% (with 30% CV) for facility soils (S1–S17), as shown in Figure 3. Table S-2 shows that OC is abundant for TSand (12.6 ± 3.6% in PM_{2.5} and 8.7 ± 3.6% in PM₁₀), OUPRd (10.8 ± 3.7% in PM_{2.5} and 11.1 ± 3.8% in PM₁₀), and FUPRd (10.2 ± 1.2% in PM_{2.5} and 13.8 ± 1.4% in PM₁₀) profiles. OC constitutes 9–11% of PM near oil sands facilities, about twice the abundance in forest soils (5–6%), as shown in Table S-3.

Figure 3 shows that one of the tailings profiles (S16) yielded the highest EC abundance (14.9% in PM_{2.5} and 10.1% in PM₁₀), possibly due to deposition from heavy-duty diesel exhaust (this is inconsistent with the other samples). Excluding S16 from the Facility profile average, EC abundances are 2–3 times higher near the oil sands operations (0.72% in PM_{2.5} and 0.52% in PM₁₀ in Facility profile) than in the more distant forest soils (0.37% in PM_{2.5} and 0.17% in PM₁₀ in Forest profile). The highway shoulder dust (S17) has a similar OC abundance (8.5 ± 0.9% of PM₁₀) compared with a paved road dust (9.5 ± 2.6% of PM₁₀) in Fresno, CA (Chow et al., 2003). However, S17 has a lower EC abundance (0.1 ± 0.1% of PM₁₀) than that from Fresno (1.7 ± 1.2% of PM₁₀). Table S-1 shows that PM₁₀ CO₃²⁻-C varies from undetectable (0.03 ± 0.28% in S10) to 3.0 ± 0.5% (mine haul road, S1). Average CO₃²⁻-C is most abundant in PM_{10-2.5}, with 0.85 ±

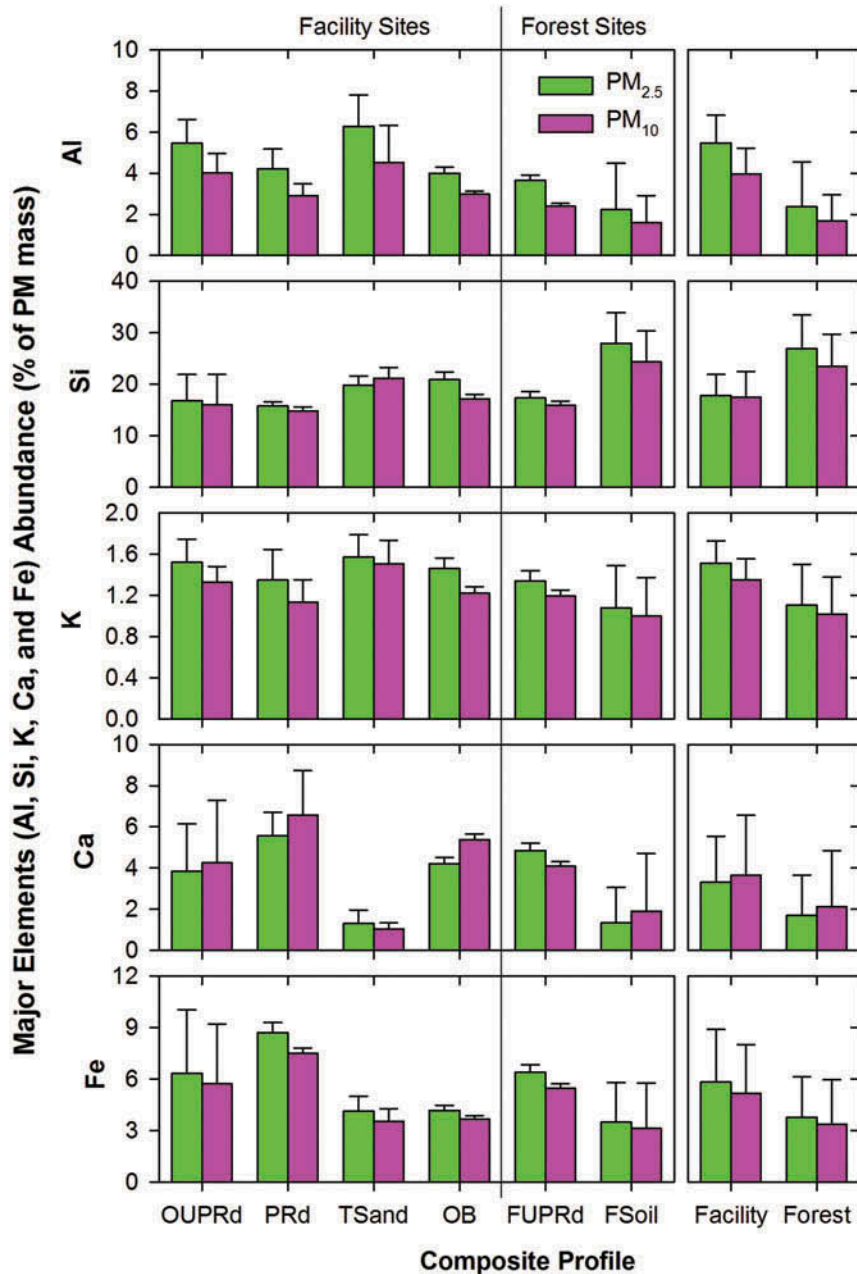


Figure 2. Composite profiles of major elements (i.e., aluminum [Al], silicon [Si], potassium [K], calcium [Ca], and iron [Fe]) with average abundance >1% in 27 PM_{2.5} and PM₁₀ samples. Emission inventory composites are facility unpaved road dust (OUPRd), paved road dust (PRd), tailings sands (TSand), overburden soil (OB), forest unpaved road (FUPRd), and forest soil (FSoil). Facility and Forest composite profiles are averages of individual profiles close to and distant from oil sands operations, respectively. Table 1 designates individual profiles included in each composite. Error bars represent the larger of standard deviation of the mean and the propagated uncertainty from the individual profiles included in the group.

1.0% in the Facility and $0.71 \pm 1.1\%$ in the Forest profiles (Table S-3).

Water-soluble ion abundances

Anion and cation abundances (Figures S-6 and S-7) vary among the samples. SO_4^{2-} is ~7 times more abundant in the Facility ($1.4 \pm 1.5\%$ of PM_{2.5} and PM₁₀) than in the Forest ($0.18 \pm 0.26\%$ of PM_{2.5} and $0.22 \pm 0.47\%$ of PM₁₀) profiles

(Figure 4). S18 is on the edge of an oil sands facility and has the highest SO_4^{2-} abundance ($0.86 \pm 0.14\%$ of PM_{2.5}) in the Forest profiles, comparable to the ~0.75% abundances at nearby facility sites (S15 and S16). The highest SO_4^{2-} abundance of 6–7% registered at a tailings pond ramp (S3).

Soluble sodium (Na^+) is also enriched in facility soils (Figure 4), particularly in the OUPRd, PRd, and TSand profiles. This is consistent with the use of wintertime deicing materials on roadways and sodium hydroxide (NaOH) to

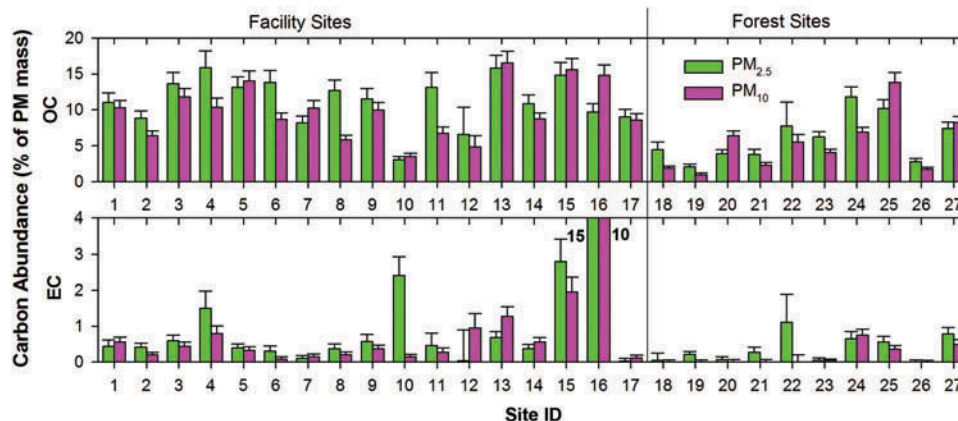


Figure 3. Organic and elemental carbon (OC and EC, respectively) abundances in individual $PM_{2.5}$ and PM_{10} profiles. Error bars represent the propagated uncertainty from the analytical and gravimetric mass uncertainties. See Table 1 for site ID.

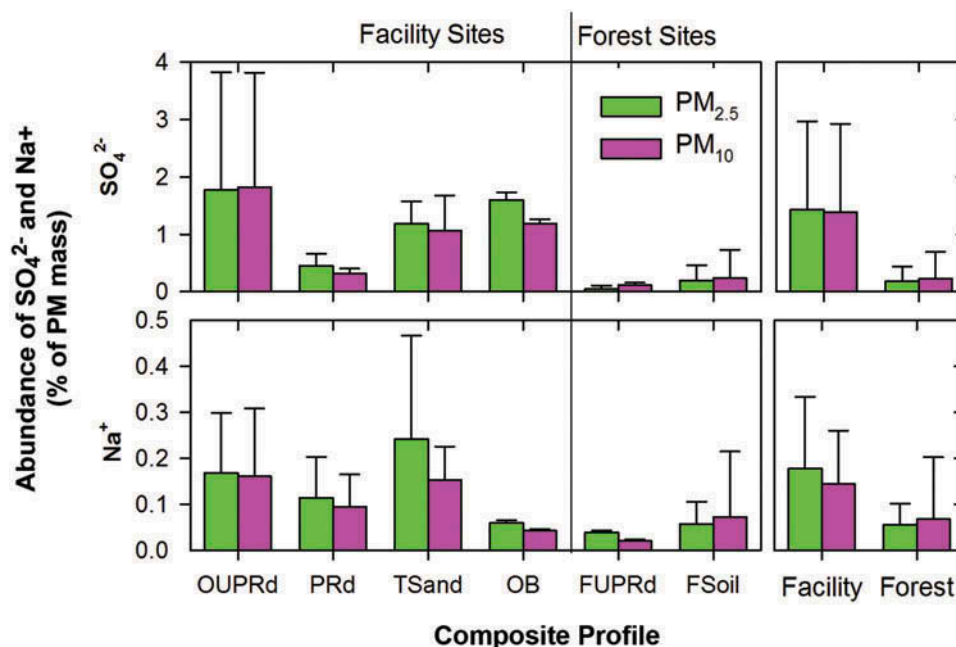


Figure 4. SO_4^{2-} and Na^+ abundances in composite $PM_{2.5}$ and PM_{10} profiles. Error bars represent the larger of standard deviation of the mean and the propagated uncertainty from the lower level profiles included in the group.

facilitate the bitumen extraction process (Tamiz Bakhtiari et al., 2015). Na^+ correlates with Cl^- ($r = 0.85$; Figure S-8a), consistent with deicing and $NaOH$ reaction with chlorinated substances. The water-soluble Ca^{2+} to total Ca ratio is nearly 1 (Figure S-8b), indicating that most of the Ca is in ionic form in most samples. This indicates that the CaO mineral assumption used for Figure 1 mass reconstruction is incomplete. The Ca^{2+}/CO_3^{2-} abundance ratio of 0.66 (Figure S-8c) is close to that of calcite ($CaCO_3$, $Ca^{2+}/CO_3^{2-} = 0.67$), which is more water-soluble than CaO . Ca^{2+} and Mg^{2+} abundances are also correlated for most profiles ($r = 0.93$; Figure S-8d), consistent with a common source (possibly dolomite, $CaMg(CO_3)_2$). The regression slope of 10.2 indicates a Ca^{2+}/Mg^{2+} molar ratio of 6.1, which is higher than the ratios of 2.4 ± 1.1 and 4.0 ± 1.5

measured from throughfall and open collectors for atmospheric deposition, respectively, in the AOSR (Watmough et al., 2014). No systematic enrichment of NH_4^+ , Mg^{2+} , and K^+ is apparent between the facility and forest soils. Sites that are believed to be affected by forest fires (i.e., S20 and S26) do not show elevated K^+ abundance (Figure S-7).

Hydrogen ion (H^+) and hydroxyl (OH^-) ions were not measured, but ion balances (Table S-8) give an indication of acidity (cation/anion < 1) or alkalinity (cation/anion > 1), which probably results from the presence of these unmeasured ions. All of the ratios in Table S-8 exceed unity, indicating that any acids that deposited on these samples were neutralized, either by atmospheric constituents or by the soils themselves. Table S-8 shows that the ratios of base cation (sum of Na^+ , Mg^{2+} , K^+ , and

Ca^{2+}) to nitrogen- and sulfur-containing ions (sum of NH_4^+ , NO_2^- , NO_3^- , and SO_4^{2-}) also exceed unity. This is consistent with AOSR measurements (Fenn et al., 2015; Watmough et al., 2014) that found atmospheric acids to be neutralized after contact with soils near oil sands operations. Because the topsoils from most sites are basic, the fugitive dusts generated from these sites are also likely to be basic, which would neutralize atmospheric acid deposition and mitigate soil acidification. The preceding analysis assumes that all the potentially acidifying species are in their final ionic forms. However, bisulfite ion (HSO_3^-), a product of sulfur dioxide (SO_2) deposition, was not distinguished from other forms in this study. The dry deposition of gaseous SO_2 , nitrogen dioxide (NO_2), nitric acid (HNO_3), and ammonia (NH_3) may also affect soil acidification.

Among the forest sites, S22 has Cl^- , NO_2^- , NO_3^- , SO_4^{2-} , NH_4^+ , and K^+ $\text{PM}_{2.5}$ abundances that are enriched by factors of 14, 46, 49, 7, 10, and 4, respectively (using lanthanum as the reference element), over relatively clean S27 that is ~100 km from major oil sands operations. Lichens at this site were blackening and dying, although no obvious signs of herbicide use were found. Lichens are sensitive to certain air pollutants, such as SO_2 and acid deposition (Gries et al., 1997; Nash and Gries, 1991). Puckett (2015) found that sulfur levels in AOSR were below the critical loads that would impair the well-being of two lichen species (i.e., *Evernia mesomorpha* and *Hypogymnia physodes*), while nitrogen deposition might be approaching levels that could affect lichen community. The enrichment of ions indicates that the soil at S22 may have been altered from its natural state, which might have led to unhealthy lichens. Short-term exposures to high concentrations of acidifying pollutants could also cause lichen damage. Further investigation is needed to identify the actual causes.

Rare earth element abundances

The 14 rare earth element abundances (Figure S-9) are similar between $\text{PM}_{2.5}$ and PM_{10} and are uniformly distributed among the facility sites, except for site S12, which has undetectable europium (Eu), gadolinium (Gd), thulium (Tm), and lutetium (Lu) in $\text{PM}_{2.5}$. The distribution is more variable among the forest sites, with S19, S20, and S22 showing the lowest and S23 (exposed soil) and S25 (surface soil) showing the highest abundances. Rare earth abundances in the Facility profile are enriched by 30–80% over the Forest profile (Table S-3).

Lead isotopes

Lead (Pb) has four stable isotopes (i.e., ^{204}Pb , ^{206}Pb , ^{207}Pb , and ^{208}Pb). ^{204}Pb is the only primordial stable isotope with a constant abundance on Earth over time, while ^{206}Pb , ^{207}Pb , and ^{208}Pb are radioactive decay products (Komárek et al., 2008). Pb sources can have distinct (sometimes overlapping) isotopic ratio ranges. Isotopic ratios are not altered by industrial/biological processes and or transport/deposition processes, so they can sometimes be used to estimate source contributions (DesJardins et al., 2004; Paulen et al., 2011; Simonetti et al.,

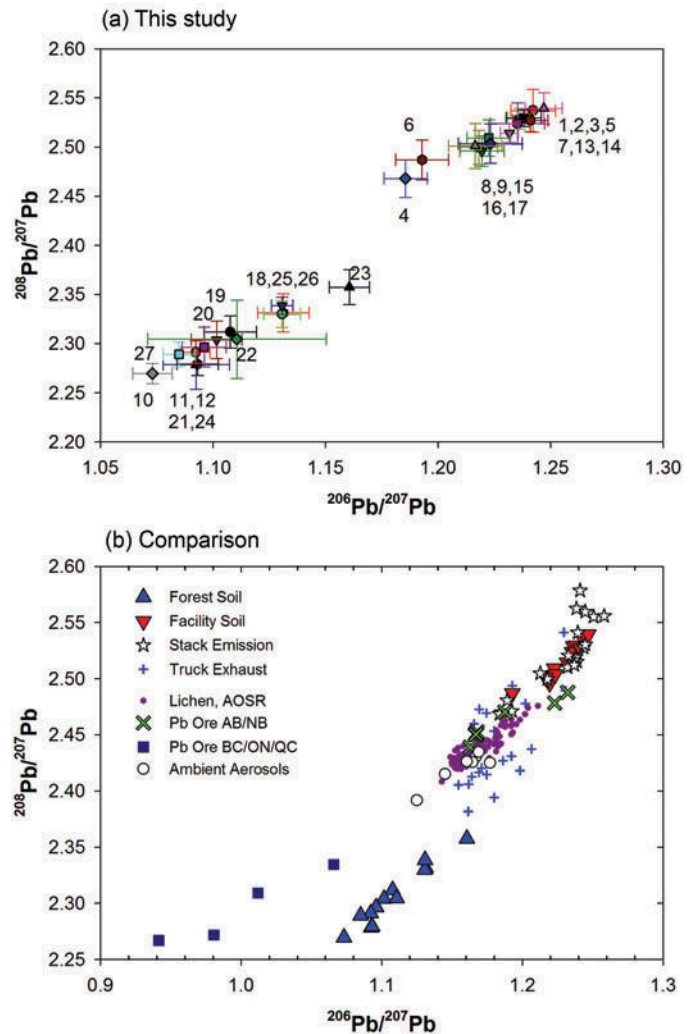


Figure 5. (a) Lead isotope ratios $^{208}\text{Pb}/^{207}\text{Pb}$ versus $^{206}\text{Pb}/^{207}\text{Pb}$ in $\text{PM}_{2.5}$ samples from this study. Number labels denote the samples described in Table 1. The upper right corner cluster includes sites in and around oil sands facilities, with $^{208}\text{Pb}/^{207}\text{Pb}$ and $^{206}\text{Pb}/^{207}\text{Pb}$ of 2.497–2.539 and 1.186–1.247, respectively; the lower left corner cluster contains most Forest sites and three Facility sites (S10–S12), with $^{208}\text{Pb}/^{207}\text{Pb}$ and $^{206}\text{Pb}/^{207}\text{Pb}$ of 2.267–2.334 and 1.070–1.142, respectively. Error bars represent the propagated uncertainty from the Pb isotope analytical uncertainties. (b) Comparison of lead isotope ratios with other studies for (1) Forest composite profile from this study (triangle); (2) Facility composite profile from this study (inverted triangle); (3) AOSR stack emissions (Watson et al., 2013a; 2013b) (unfilled star); (4) AOSR diesel haul truck emissions (Watson et al., 2013c; 2013d) (plus sign); (5) lichen samples (Graney et al., 2012) from the AOSR (small filled dot); (6) Pb-bearing minerals from northwest Alberta (Paulen et al., 2011) and New Brunswick (Cumming and Richards, 1975; Sturges and Barrie, 1987), Canada (x); (7) Pb-bearing ores from British Columbia, Ontario, and Quebec (Brown, 1962; Cumming and Richards, 1975; Sturges and Barrie, 1987) (filled square); and (8) ambient aerosols from seven Canadian cities (Burnaby, Chicoutimi, Victoria, Calgary, Winnipeg, Toronto, and New Foundland) collected from 1994 to 1999 (Bollhöfer and Rosman, 2001) (unfilled circle).

2003; Sturges and Barrie, 1987). For $\text{PM}_{2.5}$ samples, Pb isotope ratios (Figure 5a) fall into two clusters, with samples near the oil sands operations having higher $^{206}\text{Pb}/^{207}\text{Pb}$ and $^{208}\text{Pb}/^{207}\text{Pb}$ ratios than those of the more distant forest samples.

Similar clusters are found for $^{206}\text{Pb}/^{207}\text{Pb}$ and $^{204}\text{Pb}/^{206}\text{Pb}$ ratios (not shown). Three sites show ratios between the two clusters: S4 (tailings dike white sand), S6 (paved mine haul road dust), and S23 (exposed forest soil). Some of the tailings pond samples (e.g., S10–S12) have abundance ratios closer to the forest sample cluster.

Figure 5b compares $^{208}\text{Pb}/^{207}\text{Pb}$ and $^{206}\text{Pb}/^{207}\text{Pb}$ ratios from other studies, showing that AOSR stack emissions and diesel exhaust have ratios similar to those of the facility samples. AOSR lichen samples have Pb ratios similar to those of diesel exhaust and Canadian city ambient aerosols, lying in the intermediate range between the Facility and Forest profiles. Lichens obtain their nutrients from ambient air (Carignan et al., 2005). Graney et al. (2012) report Pb isotope ratios increasing with proximity to mining operations, consistent with the higher ratios near mining observed in Figure 5a. Pb isotope ratios in zinc (Zn)–Pb minerals (galena and sphalerite) collected from northwestern Alberta (Paulen et al., 2011) and in lead-bearing ores from New Brunswick (Cumming and Richards, 1975; Sturges and Barrie, 1987), Canada, are similar to those measured for diesel engine exhaust. Pb-bearing ores from British Columbia, Ontario, and Quebec, Canada, typically have much lower $^{208}\text{Pb}/^{207}\text{Pb}$ and $^{206}\text{Pb}/^{207}\text{Pb}$ ratios.

Nonpolar organic compounds

The sum of 113 nonpolar organic compounds contributed <0.1% of PM mass and <1.1% of OC with ~50% higher abundance in PM_{2.5} than PM₁₀ for most samples. The individual compounds within each functional group are summed into seven categories (Figure S-10): PAHs, lower molecular weight (MW) *n*-alkanes (C₁₅–C₂₄), higher MW *n*-alkanes (C₂₅–C₄₀), iso/anteiso-alkanes, hopanes, steranes, and others. Among the organic subgroups, lower MW *n*-alkanes (C₁₅–C₂₄) are most abundant (0.0095%), followed by hopanes (0.0077%) and higher MW *n*-alkanes (C₂₅–C₄₀; 0.0045%) in the PM_{2.5} fraction of the Facility profile (Figure 6). Only some PAHs (e.g., chrysene) and lower MW *n*-alkanes (C₁₅–C₂₄) are detectable in the forest soils (Table S-1).

The sum of 36 PAHs (0.0016–0.0025% of PM) is distributed relatively uniformly among sites, with the average ratio of Facility and Forest profiles being ~1. Tailing sands (S12) and tailing haul road dust (S16) show PAH enrichment (Figure S-10). Individual PAH abundances differ among profiles. Facility soils show abundances for almost all measured PAH species, while only a few species, notably chrysene, are abundant in the forest soils. S26 (sandy soil near unburned tree roots) has high abundances of phenanthrene, chrysene, and retene, indicating effects of biomass burning, which was evident from a charred area around the sampling location. Samples S21 (pipeline excavation soil) and S23 (exposed soil) exhibited high chrysene abundances.

n-Alkanes are abundant in all profiles, consistent with the bitumen-rich environment in the AOSR. Lower MW *n*-alkanes (C₁₅–C₂₄) (Figure S-10) distribute uniformly among facility and forest soils with a few exceptions (e.g., S12, tailing sands; and S22, unhealthy lichen forest soil). On average, higher MW *n*-alkanes (C₂₅–C₄₀) are 11.5 and 13.4 times more abundant for the facility than the

forest soils for PM_{2.5} and PM₁₀, respectively. There is a clear distinction in *n*-alkane distributions between Facility and Forest profiles (Figure S-11). *n*-Alkanes in the facility soils have bimodal or trimodal distributions, with two main peaks at C₁₅–C₁₇ and C₃₅–C₃₇, and/or a smaller peak at C₂₀–C₂₈; for the forest soils, *n*-alkanes are concentrated at C₁₅–C₂₆, with most of the higher MW *n*-alkanes being undetectable. The sums of 10 iso/anteiso-alkanes are on average 17 and 13 times more abundant for the Facility than the Forest profiles in PM_{2.5} and PM₁₀, respectively.

Hopanes and steranes are associated with bacterial and eukaryotic sources (Siljeström et al., 2010) and are used as markers for engine lubricating oils (Fraser et al., 1998). Hopanes originate from hopanepolyols present in the cell membranes of many bacteria, whereas steranes originate from sterols that modify the cell membranes of Eukaryota (Peters et al., 2005). These compounds are found in the AOSR (Brooks et al., 1988; Ram et al., 1990; Yang et al., 2011). The sums of 18 hopanes in the Facility profile are 26 and 16 times more abundant than those in the Forest profile, whereas the sums of 12 steranes in the Facility profile are 15 and 12 times more abundant for PM_{2.5} and PM₁₀, respectively. Hopane abundances are an order of magnitude higher than steranes (see Table S-3).

Several samples exhibit distinguishing features (Figure S-10). The sample from S12 (tailings pond dike sands) has higher abundances of PAHs, lower MW *n*-alkanes (C₁₅–C₂₄), methyl-alkanes (i.e., 2-methylnonadecane and 3-methylnonadecane), branched alkanes (i.e., pristane, phytane, and squalane), and cycloalkanes (i.e., octylcyclohexane, decylcyclohexane, tridecylcyclohexane, and *n*-heptadecylcyclohexane) than the other profiles, but with lower abundances for iso/anteiso-alkanes, hopanes, and steranes. Sample S22 has higher lower MW *n*-alkanes (C₁₅–C₂₄), methyl-alkanes, branched alkanes, and cycloalkanes, probably related to the unhealthy lichens at that site. Higher nonpolar compounds abundances at S25 (forest surface soil off an unpaved road) may be due to engine exhaust deposition. Sample S26, near a charred forest, contains higher PAHs, lower MW *n*-alkanes (C₁₅–C₂₄), methyl-alkanes, branched alkanes, and 1-octadecene abundances.

Carbohydrates, organic acids, and water-soluble organic carbon (WSOC)

Almost all 16 carbohydrates (Table S-1) are close to or below minimum detection limits (Table S-4) except for glycerol (0.007% of PM₁₀ at S14, ramp soil to the tailings pond dike). Formic and acetic acids are the only two detected organic acids. As shown in Figure S-12, sample S12 (tailings pond dike sand) has the highest formic and acetic acids abundances, accounting for 1.8–3.3% of PM mass and 40–51% of OC; abundances at other sites are <0.4% of PM and <10% of OC. While formic acid is not detected for several facility samples, it is detectable for most of the forest samples. Atmospheric formic acid is produced in forests by biogenic photochemical reactions and deposits to the surface (Comerford, 1990). Total WSOC accounts for 0–6% of PM and 0–66% of OC. The distribution among profiles is more uniform for the forest than the facility soils.

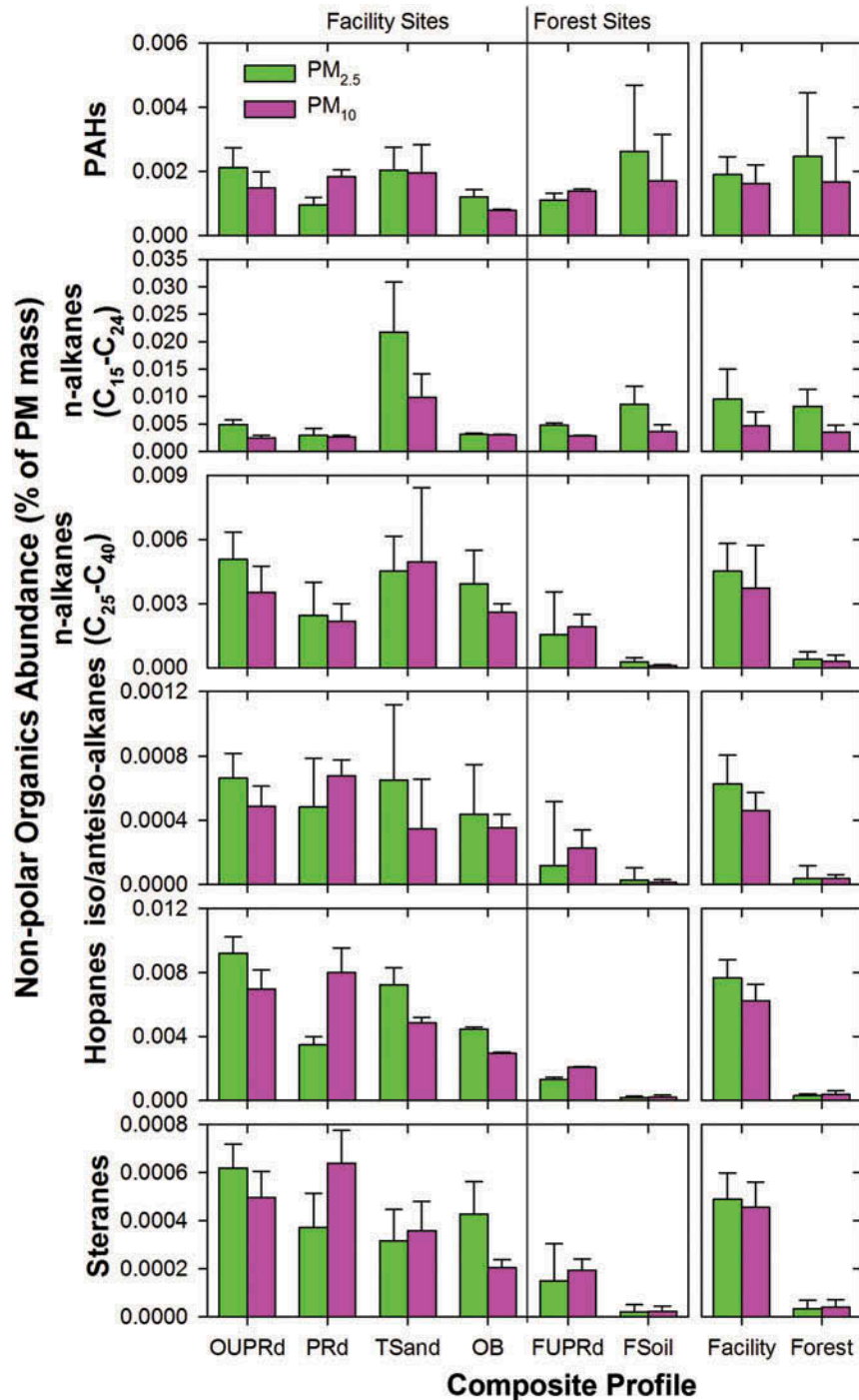


Figure 6. Nonpolar organic compound abundances in PM_{2.5} and PM₁₀ composite profiles. In order, these represent sums of (1) PAHs (polycyclic aromatic hydrocarbons); (2) low-MW *n*-alkanes (C₁₅-C₂₄); (3) high-MW *n*-alkanes (C₂₅-C₄₀); (4) iso/anteiso-alkanes; (5) hopanes; and (6) steranes. Error bars represent the larger of standard deviation of the mean and the propagated uncertainty from the lower level profiles included in the group.

Summary and Conclusion

The 27 fugitive dust samples represent a mixture of paved road dust, unpaved road dust surrounding the mining facilities and from forest roads, surface soil from excavated pits, sands from tailings ponds, mine overburden soil, and forest soil. Mass abundances of 229 chemical species, including elements

(Na to U), rare earth elements, Pb isotopes, ions, organic and elemental carbon, nonpolar organic compounds, carbohydrates, organic acids, and water-soluble organic carbon, were measured for PM_{2.5} and PM₁₀.

The five most abundant (>1% of PM) geological-related elements (i.e., Al, Si, K, Ca, and Fe) account for 25–40% of PM mass; their corresponding metal oxides in the form of

Al₂O₃, SiO₂, K₂O, CaO, and Fe₂O₃ account for 45–82% of PM mass. The most abundant geological element is Si, with 6–9% higher abundance in Forest (23–27%) than in Facility (17–18%) profiles. Average OC abundances for the Facility profile (9–11% of PM) are about twice those from the Forest profile (5–6%). Average EC abundances are 2–3 times higher in Facility (0.51–0.72% of PM) than in Forest (0.15–0.37% of PM) profiles. The ion abundances are highly variable among sites. Abundance of SO₄²⁻ is ~7 times higher in the Facility (~1.4% of PM) than in the Forest (0.18–0.24%) profiles, indicating that surface soils within and around the oils sands operations are probably contaminated by deposition of sulfur-containing compounds (e.g., S, SO₂, and SO₄²⁻) from stack emissions and engine exhaust. Good correlations were found between Na⁺ and Cl⁻, indicating the presence of NaCl. The CO₃²⁻ abundances are correlated with Ca²⁺ with a Ca²⁺/CO₃²⁻ ratio of 0.66, possibly in the form of calcite (CaCO₃, Ca²⁺/CO₃²⁻ = 0.67). The ratios of cation/anion and base cation (sum of Na⁺, Mg²⁺, K⁺, and Ca²⁺)/nitrogen- and sulfur-containing ions (sum of NH₄⁺, NO₂⁻, NO₃⁻, and SO₄²⁻) exceed unity, indicating the dusts are basic. The tailing sands profile exhibits elevated Si (19–21%), Ti (~0.6%), Zr (~0.03%), and OC (9–13%) and low Ca (~1%) and Fe (3–4%). Highest EC (10–15% PM) was found from a tailings haul road, probably due to deposition of exhaust from heavy-duty diesel engines.

Rare earth elemental abundances are similar between PM_{2.5} and PM₁₀ and among the facility sites, with 30–80% higher abundance in Facility than Forest profiles. Rare earth elements, carbohydrates, and organic acids (except for formic and acetic acids) are not useful as source markers because most of these species are below the minimum detection limits. The Pb isotope ratios (i.e., ²⁰⁸Pb/²⁰⁷Pb versus ²⁰⁶Pb/²⁰⁷Pb) show two distinct clusters, with facility soils having higher ²⁰⁶Pb/²⁰⁷Pb and ²⁰⁸Pb/²⁰⁷Pb ratios than forest soils. The close overlap of the Pb isotope ratios between the facility soil and stack emission from the AOSR indicates the soil Pb isotope ratios are probably affected by emission deposition and/or both of them are abundant in petrogenic Pb isotopes. These Pb isotopes have been used to identify industrial emissions and/or source regions.

Among the 113 nonpolar organics, lower MW *n*-alkanes (C₁₅–C₂₄) and hopanes are the most abundant species, consistent with influences in an oil-rich environment. Abundance of hopanes in PM is an order of magnitude higher than steranes. Both of those compounds reflect the influence of oil sands operations. Facility and forest soils show different *n*-alkane species distributions. On average, higher MW *n*-alkanes (C₂₅–C₄₀) are 12–13 times more abundant at facility than forest soils. The sums of 10 iso/anteiso-alkanes are on average 13–17 times more abundant at the facility than the forest soils. The sums of 18 hopanes are 16–26 times more abundant, whereas the sums of 12 steranes are 12–15 times more abundant in Facility than in Forest profiles, respectively.

Acknowledgments

This work was sponsored by the Wood Buffalo Environmental Association (WBEA), Alberta, Canada (www.wbea.org), contract

AD104-15. The content and opinions expressed by the authors in this paper do not necessarily reflect the views of WBEA or of the WBEA membership. The fugitive dust source samples were collected by Dr. Shanti Berryman, formerly with C. E. Jones & Associates, David Picard of Clearstone Engineering, Ltd, and Darrell Martindale of Shell. The authors thank Iris Saltus of the Desert Research Institute (DRI) for her help in assembling and editing the paper.

Supplemental Data

Supplemental data for this paper can be accessed at the [publisher's website](#)

References

- Addison, P.A., and K.J. Puckett. 1980. Deposition of atmospheric pollutants as measured by lichen element content in the Athabasca oil sands area. *Can. J. Bot.* 58(22):2323–34. doi:10.1139/b80-269
- Andraea, M.O. 1983. Soot carbon and excess fine potassium: Long-range transport of combustion-derived aerosols. *Science* 220:1148–51. doi:10.1126/science.220.4602.1148
- Bollhöfer, A.F., and K.J.R. Rosman. 2001. Isotopic source signatures for atmospheric lead: The Northern Hemisphere. *Geochim. Cosmochim. Acta* 65 (11):1727–40.
- Brooks, P.W., M.G. Fowler, and R.W. Macqueen. 1988. Biological marker and conventional organic geochemistry of oil sands/heavy oils, Western Canada basin. *Organic Geochem.* 12(6):519–38. doi:10.1016/0146-6380(88)90144-1
- Brown, J.S. 1962. Ore leads and isotopes. *Econ. Geol.* 57(5):673–720. doi:10.2113/gsecongeo.57.5.673
- Butler, O.T., J.M. Cook, C.M. Davidson, C.F. Harrington, and D.L. Miles. 2009. Atomic spectrometry update. Environmental analysis. *J. Anal. Atomic Spectrom.* 24(2):131–77. doi:10.1039/b821579k
- Cannon, R.E., and S.M. Anderson. 1991. Biogenesis of bacterial cellulose. *Crit. Rev. Microbiol.* 17(6):435–47. doi:10.3109/10408419109115207
- Carignan, J., G. Libourel, C. Cloquet, and L. Le Forestier. 2005. Lead isotopic composition of fly ash and flue gas residues from municipal solid waste combustors in France: Implications for atmospheric lead source tracing. *Environ. Sci. Technol.* 39(7):2018–24. doi:10.1021/es048693x
- Chow, J.C., J.G. Watson, L.C. Pritchett, W.R. Pierson, C.A. Frazier, and R.G. Purcell. 1993. The DRI Thermal/Optical Reflectance carbon analysis system: Description, evaluation and applications in U.S. air quality studies. *Atmos. Environ.* 27A(8):1185–1201. doi:10.1016/0960-1686(93)90245-T
- Chow, J.C., J.G. Watson, J.E. Houck, L.C. Pritchett, C.F. Rogers, C.A. Frazier, R.T. Egami, and B.M. Ball. 1994. A laboratory resuspension chamber to measure fugitive dust size distributions and chemical compositions. *Atmos. Environ.* 28(21):3463–3481. doi:10.1016/1352-2310(94)90005-1
- Chow, J.C., and J.G. Watson. 1999. Ion chromatography in elemental analysis of airborne particles. *Elemental Analysis of Airborne Particles, Vol. 1*, Gordon and Breach Science, Amsterdam: pp. 97–137.
- Chow, J.C., and J.G. Watson. 2002. Review of PM_{2.5} and PM₁₀ apportionment for fossil fuel combustion and other sources by the chemical mass balance receptor model. *Energy Fuels*, 16(2):222–260.
- Chow, J.C., J.G. Watson, L.L. Ashbaugh, and K.L. Magliano. 2003. Similarities and differences in PM₁₀ chemical source profiles for geological dust from the San Joaquin Valley, California. *Atmos. Environ.* 37(9-10):1317–1340. doi:10.1016/S1352-2310(02)01021-X.
- Chow, J.C., J.G. Watson, H.D. Kuhns, V.R. Etyemezian, D.H. Lowenthal, D. J. Crow, S.D. Kohl, J.P. Engelbrecht, and M.C. Green. 2004. Source profiles for industrial, mobile, and area sources in the Big Bend Regional Aerosol Visibility and Observational (BRAVO) study. *Chemosphere* 54(2):185–208.

- Chow, J.C., J.G. Watson, L.-W.A. Chen, M.-C.O. Chang, N.F. Robinson, D.L. Trimble, and S.D. Kohl. 2007a. The IMPROVE_A temperature protocol for thermal/optical carbon analysis: Maintaining consistency with a long-term database. *J. Air Waste Manage. Assoc.* 57(9):1014–23. doi:10.3155/1047-3289.57.9.1014
- Chow, J.C., J.Z. Yu, J.G. Watson, S.S.H. Ho, T.L. Bohannon, M.D. Hays, and K.K. Fung. 2007b. The application of thermal methods for determining chemical composition of carbonaceous aerosols: A review. *J. Environ. Sci. Health Part A* 42(11):1521–41. doi:10.1080/10934520701513365
- Chow, J.C., J.G. Watson, J. Robles, X.L. Wang, L.-W.A. Chen, D.L. Trimble, S.D. Kohl, R.J. Tropp, and K.K. Fung. 2011. Quality assurance and quality control for thermal/optical analysis of aerosol samples for organic and elemental carbon. *Anal. Bioanal. Chem.* 401(10):3141–3152. doi:10.1007/s00216-011-5103-3.
- Chow, J.C., D.H. Lowenthal, L.-W.A. Chen, X.L. Wang, and J.G. Watson. 2015. Mass reconstruction methods for PM_{2.5}: A review. *Air Qual. Atmos. Health* 8:243–63. doi:10.1007/s11869-015-0338-3
- Ciu, Z., Q. Liu, T.H. Etsell, J. Oxenford, and J. Coward. 2003. Heavy minerals in the athabasca oil sands tailings—Potential and recovery processes. *Can. Metallurg. Q.* 42(4):383–92.
- Comerford, N.B. 1990. Low-molecular-weight organic acids in selected forest soils of the southeastern USA. *Soil Sci. Soc. Am. J.* 54(4):1139–44.
- Cumming, G.L., and J.R. Richards. 1975. Ore lead isotope ratios in a continuously changing earth. *Earth and Planetary Science Letters*, 28(2):155–71. doi:10.1016/0012-821X(75)90223-X
- Decesari, S., M.C. Facchini, S. Fuzzi, and E. Tagliavini. 2000. Characterization of water-soluble organic compounds in atmospheric aerosol: A new approach. *J. Geophys. Res.* 105(D1):1481–89. doi:10.1029/1999JD900950
- DesJardins, M.J., K. Telmer, and S. Beauchamp. 2004. Apportioning atmospheric pollution to Canadian and American sources in Kejimikujik National Park, Nova Scotia, using Pb isotopes in precipitation. *Atmos. Environ.*, 38(39):6875–81. doi:10.1016/j.atmosenv.2004.08.039
- Dowdeswell, L., P. Dillon, S. Ghoshal, A. Miall, J. Rasmussen, and J.P. Smol. 2010. A foundation for the future: Building an environmental monitoring system for the oil sands. Canadian Ministry of the Environment, Ottawa, ON, Canada. http://www.ec.gc.ca/pollution/E9ABC93B-A2F4-4D4B-A06D-BF5E0315C7A8/1359_Oilsands_Advisory_Panel_report_09.pdf.
- Engling, G., C.M. Carrico, S.M. Kreidenweis, J.L. Collett, Jr., D.E. Day, W.C. Malm, E. Lincoln, W.M. Hao, Y. Iinuma, and H. Herrmann. 2006. Determination of levoglucosan in biomass combustion aerosol by high-performance anion-exchange chromatography with pulsed amperometric detection. *Atmos. Environ.* 40(Suppl.2):S299–311. doi:10.1016/j.atmosenv.2005.12.069
- Environment Canada. 2014. 2013 Air pollutant emissions from Alberta. Air Pollutant Emission Inventory Search, National Pollutant Release Inventory. Environment Canada, Ottawa, Ontario, Canada. http://www.ec.gc.ca/inrp-npri/donnees-data/ap/index.cfm?do=ap_result&process=true§or=&lang=en&year=2013&substance=all&location=AB&submit=Submit.
- Fenn, M.E., A. Bytnerowicz, S.L. Schilling, and C.S. Ross. 2015. Atmospheric deposition of nitrogen, sulfur and base cations in jack pine stands in the Athabasca Oil Sands Region, Alberta, Canada. *Environ. Pollut.* 196:497–510. doi:10.1016/j.envpol.2014.08.023
- Fernandez, F.J. 1989. Atomic absorption spectroscopy. In *Methods of Air Sampling and Analysis*, 83–89. Chelsea, MI: Lewis.
- Fraser, M.P., G.R. Cass, and B.R.T. Simoneit. 1998. Gas-phase and particle-phase organic compounds emitted from motor vehicle traffic in a Los Angeles roadway tunnel. *Environ. Sci. Technol.* 32(14):2051–60. doi:10.1021/es970916e
- Fung, K.K., S.L. Heisler, A. Price, B.V. Nuesca, and P.K. Mueller. 1979. Comparison of ion chromatography and automated wet chemical methods for analysis of sulfate and nitrate in ambient particulate filter samples. In *Ion Chromatographic Analysis of Environmental Pollutants*, 203–9. Ann Arbor, MI: Ann Arbor Science.
- Gargava, P., J.C. Chow, J.G. Watson, and D.H. Lowenthal. 2014. Speciated PM₁₀ emission inventory for Delhi, India. *Aerosol Air Qual. Res.* 14(5):1515–26. doi:10.4209/aaqr.2013.02.0047
- Graber, E.R., and Y. Rudich. 2006. Atmospheric HULIS: How humic-like are they? A comprehensive and critical review. *Atmos. Chem. Phys.* 6:729–53. doi:10.5194/acp-6-729-2006
- Graney, J.R., M.S. Landis, and S. Krupa. 2012. Coupling lead isotopes and element concentrations in epiphytic lichens to track sources of air emissions in the Athabasca Oil Sands Region. In *Alberta Oil Sands: Energy, Industry, and the Environment*, 343–72. Amsterdam, The Netherlands: Elsevier.
- Gries, C., M.J. Sanz, J.G. Romagni, S. Goldsmith, U. Kuhn, J. Kesselmeier, and T.H. Nash. 1997. The uptake of gaseous sulphur dioxide by non-gelatinous lichens. *N. Phytol.* 135(4):595–602. doi:10.1046/j.1469-8137.1997.00679.x
- Han, L.H., G.S. Zhuang, S.Y. Cheng, Y. Wang, and J. Li. 2007. Characteristics of re-suspended road dust and its impact on the atmospheric environment in Beijing. *Atmos. Environ.* 41:7485–99. doi:10.1016/j.atmosenv.2007.05.044
- Ho, K.F., S.C. Lee, J.C. Chow, and J.G. Watson. 2003. Characterization of PM₁₀ and PM_{2.5} source profiles for fugitive dust in Hong Kong. *Atmos. Environ.* 37(8):1023–32. doi:10.1016/S1352-2310(02)01028-2
- Ho, S.S.H., and J.Z. Yu. 2004. Determination of airborne carbonyls: Comparison of a thermal desorption/GC method with the standard DNPH/HPLC method. *Environ. Sci. Technol.* 38(3):862–70. doi:10.1021/es034795w
- Jacobs, F.S., and R.H. Filby. 1982. Trace element composition of Athabasca tar sands and extracted bitumens. In *Atomic and Nuclear Methods in Fossil Energy Research*, 49–59. New York, NY: Springer.
- Jaffrezo, J.L., N. Calas, and M. Bouchet. 1998. Carboxylic acid measurements with ionic chromatography. *Atmos. Environ.* 32(14/15):2705–8. doi:10.1016/S1352-2310(98)00026-0
- Kelly, E.N., J.W. Short, D.E. Schindler, P.V. Hodson, M.S. Ma, A.K. Kwan, and B.L. Fortin. 2009. Oil sands development contributes polycyclic aromatic compounds to the Athabasca River and its tributaries. *Proc. Natl. Acad. Sci. USA* 106(52):22346–51. doi:10.1073/pnas.0912050106
- Kelly, E.N., D.E. Schindler, P.V. Hodson, J.W. Short, R. Radmanovich, and C. C. Nielsen. 2010. Oil sands development contributes elements toxic at low concentrations to the Athabasca River and its tributaries. *Proc. Natl. Acad. Sci. USA* 107(37):16178–83. doi:10.1073/pnas.1008754107
- Komárek, M., V. Ettler, V. Chrastný, and M. Mihaljevic. 2008. Lead isotopes in environmental sciences: A review. *Environ. Int.* 34(4):562–77. doi:10.1016/j.envint.2007.10.005
- Kunzig, R. 2009. The Canadian oil boom: Scraping bottom. *Natl. Geogr.* 215(3):34–59.
- Landis, M.S., J.P. Pancras, J.R. Graney, R.K. Stevens, K.E. Percy, and S. Krupa. 2012. Receptor modeling of epiphytic lichens to elucidate the sources and spatial distribution of inorganic air pollution in the Athabasca Oil Sands Region. In *Alberta Oil Sands: Energy, Industry, and the Environment*, 427–67. Amsterdam, The Netherlands: Elsevier.
- Morman, S.A., and G.S. Plumlee. 2013. The role of airborne mineral dusts in human disease. *Aeolian Res.* 9:203–12. doi:10.1016/j.aeolia.2012.12.001
- Nash, T.H., and C. Gries. 1991. Lichens as indicators of air pollution. In *Air Pollution*, 1–29. Berlin, Germany: Springer.
- Ohno, T., and T. Hirata. 2004. Advances in elemental and isotopic analyses by ICP-mass spectrometry and their applications to geochemistry. *Bunseki Kagaku* 53(7):631–44. doi:10.2116/bunsekikagaku.53.631
- Pant, P., and R.M. Harrison. 2013. Estimation of the contribution of road traffic emissions to particulate matter concentrations from field measurements: A review. *Atmos. Environ.* 77:78–97. doi:10.1016/j.atmosenv.2013.04.028
- Paulen, R.C., S. Paradis, A. Plouffe, and I.R. Smith. 2011. Pb and S isotopic composition of indicator minerals in glacial sediments from NW Alberta, Canada: Implications for Zn-Pb base metal exploration. *Geochemistry Explor. Environ. Anal.* 11(4):309–20. doi:10.1144/1467-7873/10-IM-032
- Peters, K.E., C.C. Walters, and J.M. Moldovan. 2005. *The Biomarker Guide: II. Biomarkers and Isotopes in Petroleum Systems and Earth History*. Cambridge, UK: Cambridge University Press.
- Pitchford, M.L., W.C. Malm, B.A. Schichtel, N.K. Kumar, D.H. Lowenthal, and J.L. Hand. 2007. Revised algorithm for estimating light extinction from IMPROVE particle speciation data. *J. Air Waste Manage. Assoc.* 57(11):1326–36. doi:10.3155/1047-3289.57.11.1326

- Pribyl, D.W. 2010. A critical review of the conventional SOC to SOM conversion factor. *Geoderma* 156(3–4):75–83. doi:10.1016/j.geoderma.2010.02.003
- Puckett, K. 2015. Chemical composition and lichen community change in the AOSR. In *Assessing Forest Health in the Athabasca Oil Sands Region—WBEA Report # 2015-05-25*, 145–66. Fort McMurray, AB, Canada: Wood Buffalo Environmental Association.
- Puttaswamy, N., and K. Liber. 2012. Influence of inorganic anions on metals release from oil sands coke and on toxicity of nickel and vanadium to *Ceriodaphnia dubia*. *Chemosphere* 86(5):521–29. doi:10.1016/j.chemosphere.2011.10.018
- Ram, S., D.K. Saraswat, and K.A. Narayan. 1990. Spectroscopic studies of Athabasca oil sands. *Fuel* 69(4):512–15. doi:10.1016/0016-2361(90)90324-J
- Schulten, H.R., and P. Leinweber. 2000. New insights into organic-mineral particles: Composition, properties and models of molecular structure. *Biol. Fertil. Soils* 30(5–6):399–432. doi:10.1007/s003740050020
- Shafer, M.M., B.M. Toner, J.T. Oyerdier, J.J. Schauer, S.C. Fakra, S.H. Hu, J. D. Herner, and A. Ayala. 2012. Chemical speciation of vanadium in particulate matter emitted from diesel vehicles and urban atmospheric aerosols. *Environ. Sci. Technol.* 46(1):189–95. doi:10.1021/es200463c
- Siljeström, S., J. Lausmaa, P. Sjövall, C. Broman, V. Thiel, and T. Hode. 2010. Analysis of hopanes and steranes in single oil-bearing fluid inclusions using time-of-flight secondary ion mass spectrometry (ToF-SIMS). *Geobiology* 8(1):37–44.
- Simonetti, A., C. Garipey, and J. Carignan. 2003. Tracing sources of atmospheric pollution in Western Canada using the Pb isotopic composition and heavy metal abundances of epiphytic lichens. *Atmos. Environ.* 37(20):2853–65. doi:10.1016/S1352-2310(03)00210-3
- Stringham, G. 2012. Energy developments in Canada's oil sands. In *Alberta Oil Sands: Energy, Industry, and the Environment*, 19–34. Amsterdam, The Netherlands: Elsevier.
- Studabaker, W.B., S. Krupa, R.K.M. Jayanty, and J.H. Raymer. 2012. Measurement of polynuclear aromatic hydrocarbons (PAHs) in epiphytic lichens for receptor modeling in the Athabasca Oil Sands Region (AOSR): A pilot study. In *Alberta Oil Sands: Energy, Industry, and the Environment*, 391–425. Amsterdam, The Netherlands: Elsevier.
- Sturges, W.T., and L.A. Barrie. 1987. Lead 206/207 isotope ratios in the atmosphere of North America as tracers of US and Canadian emissions. *Nature* 329(6135):144–46. doi:10.1038/329144a0
- Tamiz Bakhtiari, M., D. Harbottle, M. Curran, S. Ng, J. Spence, R. Siy, Q. Liu, J. Masliyah, and Z.H. Xu. 2015. Role of caustic addition in bitumen-clay interactions. *Energy Fuels* 29(1):58–69. doi:10.1021/ef502088z
- Thorpe, A., and R.M. Harrison. 2008. Sources and properties of non-exhaust particulate matter from road traffic: A review. *Sci. Total Environ.* 400(1–3):270–82. doi:10.1016/j.scitotenv.2008.06.007
- U.S. Environmental Protection Agency. 1997. Appendix L to Part 50 - Reference method for the determination of fine particulate matter as PM_{2.5} in the atmosphere. *Fed. Reg.* 62(138):57–95.
- Vega, E., V. Mugica, E. Reyes, G. Sanchez, J.C. Chow, and J.G. Watson. 2001. Chemical composition of fugitive dust emitters in Mexico City. *Atmos. Environ.* 35(23):4033–39. doi:10.1016/S1352-2310(01)00164-9
- Watmough, S.A., C.J. Whitfield, and M.E. Fenn. 2014. The importance of atmospheric base cation deposition for preventing soil acidification in the Athabasca Oil Sands Region of Canada. *Sci. Total Environ.* 493:1–11. doi:10.1016/S1352-2310(01)00164-9
- Watson, J.G., J.C. Chow, and C.A. Frazier. 1999. X-ray fluorescence analysis of ambient air samples. In *Elemental Analysis of Airborne Particles, Vol. 1*, 67–96. Amsterdam, The Netherlands: Gordon and Breach.
- Watson, J.G., B.J. Turpin, and J.C. Chow. 2001. The measurement process: Precision, accuracy, and validity. In *Air Sampling Instruments for Evaluation of Atmospheric Contaminants*, 9th ed., 201–16. Cincinnati, OH: American Conference of Governmental Industrial Hygienists.
- Watson, J.G., J.C. Chow, X.L. Wang, S.D. Kohl, and D.A. Sodeman. 2013a. Measurement of real-world stack emissions in the Athabasca Oil Sands Region with a dilution sampling system during August, 2008. Reno, NV: Desert Research Institute.
- Watson, J.G., J.C. Chow, X.L. Wang, S.D. Kohl, S. Gronstal, and B. Zielinska. 2013b. Measurement of real-world stack emissions in the Athabasca Oil Sands Region with a dilution sampling system during March, 2011. Reno, NV: Desert Research Institute.
- Watson, J.G., J.C. Chow, X.L. Wang, D.H. Lowenthal, S.D. Kohl, and S. Gronstal. 2013c. Characterization of real-world emissions from nonroad mining trucks in the Athabasca Oil Sands Region during October, 2010. Reno, NV: Desert Research Institute.
- Watson, J.G., J.C. Chow, X.L. Wang, B. Zielinska, S.D. Kohl, and S. Gronstal. 2013d. Characterization of real-world emissions from nonroad mining trucks in the Athabasca Oil Sands Region during September, 2009. Reno, NV: Desert Research Institute.
- Watson, J.G., and J.C. Chow. 2015. Receptor models and measurements for identifying and quantifying air pollution sources. In *Introduction to Environmental Forensics*, 3rd ed., 677–706. Amsterdam, The Netherlands: Elsevier.
- Weinhold, B. 2011. Alberta's oil sands: Hard evidence, missing data, new promises. *Environ. Health Perspect.* 119(3):126–31. doi:10.1289/ehp.119-a126
- Wu, F., J.C. Chow, Z.S. An, J.G. Watson, and J.J. Cao. 2011. Size-differentiated chemical characteristics of Asian Paleo dust: Records from aeolian deposition on the Chinese loess plateau. *J. Air Waste Manage. Assoc.* 61(2):180–89. doi:10.3155/1047-3289.61.2.180
- Yang, C., Z.D. Wang, Z.Y. Yang, B. Hollebone, C.E. Brown, M. Landriault, and B. Fieldhouse. 2011. Chemical fingerprints of Alberta oil sands and related petroleum products. *Environ. Forens.* 12(2):173–88. doi:10.1080/15275922.2011.574312

About the Authors

Xiaoliang Wang is an associate research professor at the Desert Research Institute, Nevada System of Higher Education, in Reno, NV.

Judith C. Chow and **John G. Watson** are research professors at the Desert Research Institute, Nevada System of Higher Education, in Reno, NV.

Steven D. Kohl is an associate research scientist at the Desert Research Institute, Nevada System of Higher Education, in Reno, NV.

Kevin E. Percy is the executive director of the Wood Buffalo Environmental Association (WBEA) in Fort McMurray, Alberta, Canada.

Allan H. Legge is a senior science advisor to the Wood Buffalo Environmental Association (WBEA) in Fort McMurray, Alberta, and president of Biosphere Solutions in Calgary, Alberta, Canada.